Exploring statistical complexity and enabling speckle-free imaging with Dye-Kaolinite colloidal random lasers

P.K. Nideesh, R. Antoine, N. Kalarikkal

Exploring statistical complexity and enabling speckle-free imaging with Dye-Kaolinite colloidal random lasers

P. K. Nideesh[1], R. Antoine[2], and N. Kalarikkal [1,3,4*]

[1]School of Pure and Applied Physics, Mahatma Gandhi University, Kottayam-686 560, Kerala, India

[2]Institut Lumière Matière UMR 5306, Univ Lyon, Université Claude Bernard Lyon 1, CNRS, F-69100 Villeurbanne, France

[3]International Centre for Ultrafast Studies, Mahatma Gandhi University, Kottayam-686 560, Kerala, India

[4]International and Inter University Centre for Nanoscience and Nanotechnology, Mahatma Gandhi University, Kottayam-686 560, Kerala, India

[*]Corresponding author Email: nkalarikkal@mgu.ac.in

Abstract

This article extends our previous investigation into random lasers (RLs), focusing on the incorporation of Rhodamine 6G (R6G) dye in methanol with Kaolinite nanoclay scatterers as a disordered active medium for colloidal RLs. Building upon the prior exploration, which specifically focused on understanding the performance dependence related to the concentration of gain medium and scatterers, this report takes a closer look. It conducts a thorough statistical analysis of the incoherent dye-Kaolinite random lasing spectra, particularly in the context of replica symmetry breaking (RSB) and Lévy statistics. This study highlights that RSB was observed around the threshold energy and can serve as an indicator of the threshold. Gaussian distribution prevailed below, near, and far above the lasing threshold estimated from the levy (α) exponent, suggesting the absence of Lévy flight behavior. Additionally, Pearson correlation coefficients (PCC) were used to quantify the correlation between intensity fluctuations at different wavelengths, with the results visually represented by heatmaps. Furthermore, the random lasing output was utilized to achieve speckle-free imaging.

1 Introduction

The concept of RLs involves the generation of laser-like emission without the need for conventional optical cavities or mirrors [1]. Instead, RLs utilize multiple scattering events within a disordered

medium to achieve feedback and amplify light [2–6]. This unique approach to lasing offers several advantages and has gained significant interest in various fields of research [6, 7]. Their flexibility in choosing materials and configurations allows for the development of compact and cost-effective laser-like sources. It also exhibits remarkable tolerance to disorder and can operate in highly scattering and disordered media, including powders [8–10], polymers [11–13] colloids [14–16] and biological tissues [17–19]. RLs provide opportunities for exploring the notions of statistical physics like spin glass (SG), Lévy statistics, Floquet SG phase and turbulence [20–23]. These studies contribute to our understanding of the behavior of light in complex and disordered systems and lead to advancements in areas like condensed matter physics and optical engineering.

A noteworthy characteristic of RLs lie in their notable parallels with the intricate domain of thermodynamic SG. Despite being distinct sectors within the realms of photonics and condensed matter physics, RLs and SG [20, 24, 25] have recently unveiled unforeseen associations, elucidating shared underlying physics. Both disciplines are intrinsically linked through the framework of RSB [26, 27, 24]. RSB is a theoretical concept rooted in statistical physics, particularly applied to disordered systems like spin glasses. The idea of RSB is that identical systems prepared in the same way may yield different experimental measurements, due to being trapped in distinct minima within the free energy landscape for extended periods. Parisi's seminal idea of RSB has had a profound impact not only on the understanding of disordered magnetic systems but also across various branches of physics and other scientific fields [26, 28–33]. One significant manifestation of RSB is its role in elucidating the transition from paramagnetic to SG phases in the magnetic domain. The pioneering work of Ghofraniha et al. in 2015 provided the initial experimental evidence of a photonic paramagnetic to SG phase transition in RLs [24].

In SG, the magnetic moments of individual spins engage in disordered interactions, giving rise to complex energy landscapes and the emergence of multiple equilibrium states. In RLs, modes are conceptualized as spin variables, with the excitation energy effectively playing the role of inverse temperature [24]. When the pump intensity remains low (indicating high temperatures), the RL modes can be independently excited owing to the sufficient optical gain available within the system. However, as the pump intensity increases (representing lower temperatures), the RL modes engage in competition for survival due to the reduced gain within the system. At higher pump intensities, the RL modes undergo correlated oscillations driven by strong intermodal coupling facilitated by nonlinearity and disorder. It is crucial to emphasize that previous studies have highlighted the significant role of mode interaction as a key factor influencing the occurrence of RSB in a lasing device [34–38].

The observation of RSB in RLs has sparked considerable interest, opening new avenues for understanding these fascinatingly chaotic light sources. However, questions remain about the applicability of RSB analysis to liquid-phase RLs, characterized by inherent time-dependent fluctuations due to Brownian motion. In 2016, Pincheira et al. studied RSB in specially designed amorphous TiO_2 particles suspended in an ethanol-R6G solution (an incoherent RL) [39]. Additionally, Tommasi et al., in 2016, used a ZnO-dye solution RL, and this study observed time-dependent speckle fluctuations, highlighting the non-quenched disorder in liquid systems. Their study focused on the dynamic nature of liquid materials, revealing speckle movements between consecutive shots [40]. P K Nideesh et al. showed RSB from the colloidal sample using R6G as a gain medium and potassium sodium niobate as a scatterer [15].

One of the most peculiar features of RLs is its output intensity fluctuations. The investigation into output intensity fluctuations initially focused on analyzing probability distributions. D Sharma et al., in 2006, explained dominating intensity fluctuations due to the presence of rare, long-lived extended modes that exceed the amplification length that can lead to intensity fluctuations. This behavior is observed in various experiments and attributed to the Lévy intensity distribution in RLs [41]. Lepri et al., in 2007, explored the statistical regimes within RLs, introducing a diffusive model that links emission probability to gain and the mean free path length of scattering [42]. The Lévy exponent (α) in this diffusive regime serves as a critical factor, determining a transition from a Gaussian ($\alpha > 2$) to a Lévy distribution ($\alpha \leq 2$), particularly in proximity to the RL threshold. R. Uppu et al. introduced a method employing the α-stable distribution to assess the statistical regime of intensity fluctuation in RLs [43–45]. Their work demonstrated that RL intensity fluctuations follow Lévy statistics around the threshold pump power, with the Lévy exponent serving as a universal identifier of the threshold.

In RLs, fluctuations in emitted intensity have been shown to exhibit Lévy-like behavior near the lasing threshold, reflecting strong emission fluctuations due to large gain variations and disorder [42, 46]. The studies of Gomes et al. (2016), which compared the transition from Gaussian to Lévy regimes and the RSB glassy phase near the RL threshold [47]. We observe that the onset of the RL threshold is marked by a shift from Gaussian fluctuations ($\alpha = 2$) to Lévy-type statistics ($0 < \alpha < 2$), supporting the notion that Lévy flights play a key role in light transport during the RSB transition. This is further demonstrated by the extreme fluctuations in the emission spectra close to the threshold, which correspond to the emergence of Lévy distributions and the photonic spin-glass state. The onset of the Lévy statistical regime of intensity fluctuations and the emergence of the RSB glassy RL phase has also been recently reported in a one-dimensional Er-RFL by Lima et al. [48]. However, our current findings on R6G dye in methanol and Kaolinite nanoclay RL systems indicate the presence of RSB without any sign of Lévy flight. The absence of Lévy behavior can be attributed to the tendency of fluctuations to cluster around a mean value, resulting in finite variance and supporting the continued prevalence of Gaussian statistics in this context. The results support the observations of Tommasi et al. (2016), who suggested that while RSB and Lévy statistics can coincide near the RL threshold, they are not always causally linked [40]. It finds that the Lévy regime dominates near the threshold where large fluctuations in the gain medium are prominent. Interestingly, recent studies on Förster resonance energy transfer (FRET)-assisted RLs have also highlighted a different dynamic [49]. In such systems, FRET induces disorder and frustrates coherent mode oscillations, leading to a discrete emission field with low spatiotemporal coherence. This suggests that while Lévy flights dominate near the lasing threshold in certain RL systems, alternative mechanisms like FRET can influence emission characteristics in ways that differ from typical Lévy or Gaussian statistical behavior.

Speckle-free imaging is a key application of RLs, made possible by their inherent lack of spatial coherence, which effectively reduces speckle noise and enhances imaging quality. Recent advancements in RLs have significantly improved their potential for speckle-free imaging by utilizing innovative materials and technologies. For instance, programmable pumping strategies have enabled on-demand color lasing with directional emission in fiber-integrated systems, making them suitable for imaging applications [50]. Surface-emitting perovskite random lasers (SERLs) have demonstrated low spatial coherence and narrow divergence angles, effectively

suppressing speckle noise, offering promising solutions for integrated imaging systems [51, 52]. The incorporation of quasi-2D perovskite films and adipic acid has further reduced lasing thresholds and improved brightness, underscoring their potential for high-quality imaging [53] . Flexible RLs based on perovskite quantum dots have also demonstrated robustness in maintaining performance under mechanical stress, while high-power multimode random fiber lasers have achieved impressive reductions in speckle contrast, enhancing imaging performance [54, 55]. In addition, advances such as dual-color plasmonic RLs and those enhanced by titanium nitride nanoparticles have pushed the boundaries of low-threshold lasing and speckle-free imaging in complex environments [56, 57]. Several studies have utilized natural and biological materials, such as butterfly wings and bamboo leaves, as scatterers in RLs, showcasing cost-effective solutions for sustainable, speckle-free imaging [58, 59]. These developments highlight the significant progress in reducing speckle noise, making RLs promising candidates for biomedical imaging, optoelectronic devices, and full-field imaging applications [60, 61].

This report expands on our previous studies which examine the effects of gain and scatterer concentration in R6G-Kaolinite nanoclay RLs [14]. Here, we present the results of a statistical analysis focusing on RSB to understand the random lasing behavior. Additionally, we investigated whether the output intensity fluctuations exhibit characteristics of Lévy flight dynamics. PCC was calculated to quantify the degree of correlation between intensity fluctuations at different wavelengths, and corresponding heatmaps were generated for visualization. Further, the utility of the RL output by achieving speckle-free imaging of a transmission electron microscope (TEM) grid was demonstrated.

2 Experimental details

The experimental setup used for RL characterization was the same as described in the previous work [14]. Briefly, a Q-switched Nd:YAG laser operating at 1 Hz, with a wavelength of 532 nm and a pulse duration of 6 ns, was used as the excitation source. The laser beam was focused onto the sample using a lens with a focal length of 10 cm, resulting in a beam diameter of approximately 100 μm. The materials employed included an active medium [R6G (5 mM)] and scatterers [Kaolinite nanoclay (20 mg/ml)] within the dye medium. To prepare the sample, R6G dye and nanoclay were mixed in a solution, ensuring even distribution of the scatterers by ultrasonication and then followed by continuous magnetic stirring throughout the experimental time frame. The RL emission was collected and focused onto a fiber-coupled spectrometer (Andor SR-500i spectrograph) using a collection optics setup. The signal was detected using an intensified charge-coupled device (ICCD, Andor iStar). Single-shot nanosecond spectral measurements were performed for RL analysis.

3 Results and discussion

3.1 Basic random lasing characterization

A previous investigation [14] on the characterization of dye Kaolinite nanoclay-based RLs revealed several key findings. The line width narrowing of the RL spectra was observed to be

approximately 5 nm above a threshold pump energy of 40 μJ per pulse, which indicated the onset of lasing behavior in the system. It could be understood from the intensity dependence of the emission as a function of pump energy. A significant increase in output intensity was observed beyond the threshold. Moreover, the threshold behavior of the RL showed a clear transition from spontaneous emission to incoherent RL emission at the established threshold. Also narrowing and beta factors are calculated for a thorough understanding of the system. These findings collectively indicated the successful realization of random lasing in the system, utilizing the combination of R6G dye and Kaolinite nanoclay as scatterers.

3.2 Photonic replica symmetry breaking studies

The current analysis was focused on investigating RSB in the context of an incoherent (smooth narrow spectrum) random lasing scheme. In the case of an incoherent RL, where phase information is not preserved, the emission spectrum does not exhibit wavelength dependence [62, 63]. Instead, it forms a Gaussian-like emission profile centered around the maximum of the spontaneous emission band, corresponding to the modes with the highest gain within the system, a phenomenon well discussed in literature [1, 64]. The spatial overlap of these modes promotes interaction among them, leading to increased spectral correlation. This interaction has the effect of favoring modes at frequencies where the system has greater available gain. Consequently, the emission spectrum exhibits a smooth, single-peak characteristic of incoherent emission.

The Parisi overlap parameter ($q_{\alpha\beta}$) is estimated to quantify RSB in the context of RLs and can be expressed as [24, 15]:

$$q_{\alpha\beta} = \frac{\sum_{k=1}^{N} \triangle_\alpha(k)\triangle_\beta(k)}{\sqrt{\sum_{k=1}^{N} \triangle_\alpha^2(k)}\sqrt{\sum_{k=1}^{N} \triangle_\beta^2(k)}} \tag{1}$$

where α and β represent replica labels, ranging from 1 to N typically, with N being the number of system replicas and is often 230 in this case. These replicas are binned on a size of 0.04 nm, which is motivated by the need to strike a balance between capturing fine-scale fluctuations in the replica order parameters and mitigating the effects of inherent noise within the system. The terms $\triangle_\alpha(k)$ and $\triangle_\beta(k)$ signify the intensity fluctuation of the α^{th} and β^{th} replica at a specific wavelength indexed as k and is defined as [24, 15]:

$$\triangle_\alpha(k) = I_\alpha(k) - \bar{I}(k) \tag{2}$$

$\bar{I}(k)$ is the mean intensity of a mode within a RL at a specific wavelength indexed as k and can be computed as:

$$\bar{I}(k) = \sum_{\alpha=1}^{N} I_\alpha(k)/N \tag{3}$$

It is important to note that the investigations into RSB in RLs have predominantly centered around the assumption that disorder is quenched, implying that it does not change over time. However, achieving complete quenched disorder and identical realization conditions is challenging in colloidal RLs. Recent findings, as reported by Pincheira et al. (2016) and Tommasi et al. (2016), have indicated the occurrence of RSB even in liquid RLs [65, 40]. According to Tommasi

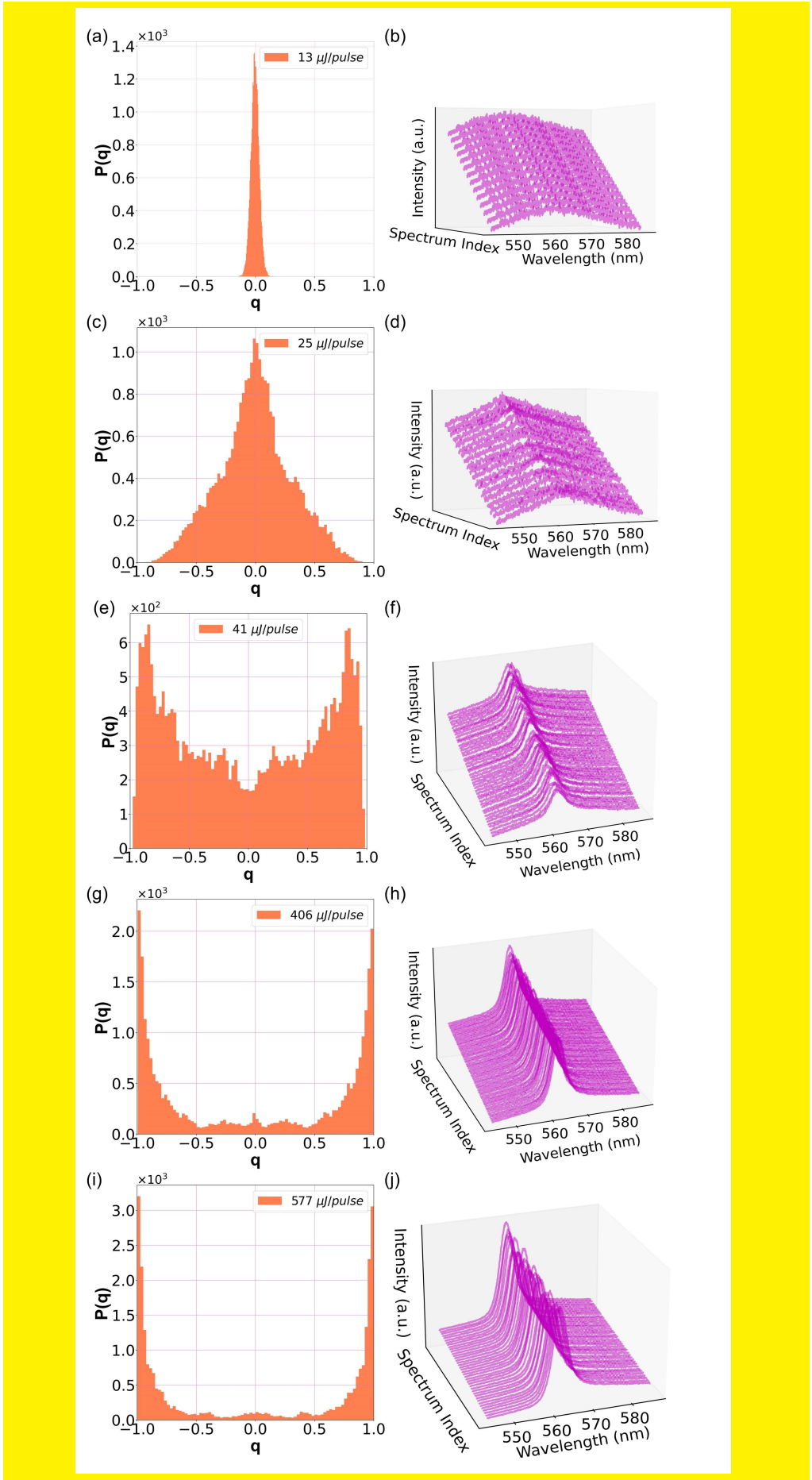

Figure 1: Probability distribution functions of the overlap ($P(q)$) for R6G-Kaolinite RL (a, c, e, g, and i), with the pump energies shown in the inset. The corresponding indicative spectra are presented in panels (b, d, f, h, and j).

et al., RSB is a general phenomenon connected to the threshold of the RL [40], and it is associated with the threshold irrespective of whether the intensity fluctuations fall under Lévy or Gaussian regime [40]. Even though an ensemble of different disorder configurations are considered, it is worth mentioning that each measurement could be considered quenched at the time scales of individual data acquisition. Also, the scatterer motion can be regarded as frozen in the RL lifetime so that the condition of identical disorder realization can be fulfilled to a large extent. By examining the probability distribution function (PDF) of an order parameter known as Parisi overlap (q), it is possible to determine the effect of RSB [26].

To analyze the PDF, the intensity fluctuations at 5 different excitation energies are computed, as shown in Figs. 1a, 1c, 1e, 1g, and 1i. These specific energy values were strategically chosen to span critical points (threshold), peaks and transitions (fluorescence to RL) that ensured a systematic investigation of the response of the RL system (a more detailed representation of Fig. 1 is presented in S1). Fig. 1 clearly demonstrates that the symmetry among replicas is broken around a threshold energy level of 40 μJ per pulse. The shape of the PDF ($P(q)$) plays a crucial role in determining whether there is symmetry breaking or not. This statistical analysis enhances the knowledge of RLs in terms of pulse-to-pulse intensity variations. The critical parameter of concern is the value of q at which $P(q)$ attains its peak denoted as q_{max}. RSB commences around the threshold and is evident from the findings shown in Fig. 1. This close association between the RSB transition and the lasing threshold is reported in literature [65, 40]. Before reaching the threshold, at lower pump energy levels, the PDF peaks at $q = 0$ ($q_{max} = 0$), as shown in Fig. 1a. Notably, even at energies significantly above the threshold, the overall shape of the PDF remains similar, reflecting a photonic SG like phase. Specifically, the peak of the PDF shifts towards $|q| = 1$ ($q_{max} = 1$), as seen in Figs. 1e, 1g, and 1i. This behavior indicates the

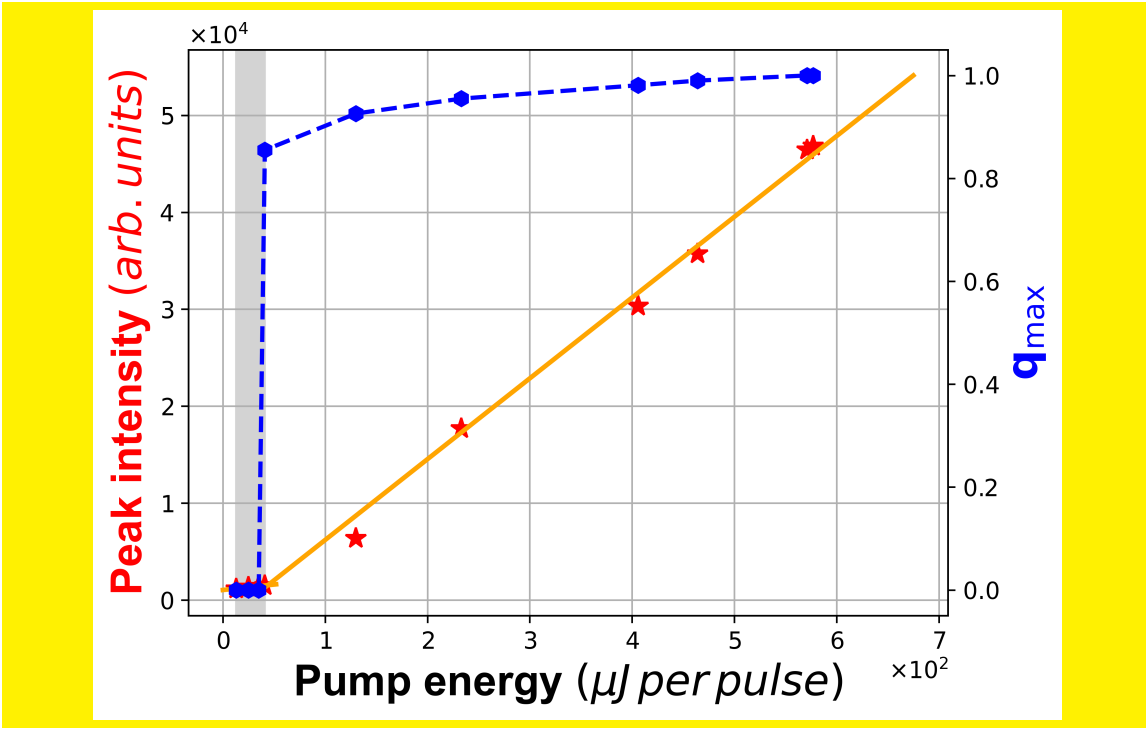

Figure 2: Plot depicting the variation of the maximum overlap value (q_{max}) and peak intensity with respect to pump energy.

correlated oscillation of modes within the RL system and suggests the occurrence of a photonic

SG transition phase. The corresponding spectra is shown in the right pannel of Fig 1 (Figs. 1b, 1d 1f, 1h and 1j). The correlation, in this case, arises from the interaction between different lasing modes within the random scattering medium. These interactions cause the modes to synchronize their oscillations, leading to the emergence of a collective behavior that persists even at high excitation energies. The occurrence of RSB and the subsequent interaction of RL modes highlight the complex nature of the system as it shift from a regime dominated by spontaneous emission to the one characterized by random lasing emission. The variations in the magnitude of q_{max} and peak intensity with pump energy is demonstrated in Fig. 2. It indicates that the value of q_{max} underwent a significant change at the threshold point (from zero to a higher value near 1). The presence of RSB can be regarded as a significant manifestation of the threshold energy since it occurs around the threshold. These findings represent a substantial advancement in the perception of the emergence of RSB in the specific context of incoherent liquid or colloidal RLs. The established association between RSB and the lasing threshold not only validates previous experimental observations but also introduces a novel facet to this scientific inquiry when applied to the specific domain of dye-Kaolinite colloidal RLs.

3.3 Pearson correlation heatmaps

Another potential method for exploring correlations involves the utilization of Pearson correlation heatmaps that offer a visual representation of the associations among variables, facilitating a more profound comprehension of their interconnections. PCC denoted as $C(\lambda_j, \lambda_k)$ is employed to evaluate the link between intensity fluctuations at distinct wavelengths ($I(\lambda_j)$ and $I(\lambda_k)$). $C(\lambda_j, \lambda_k)$ is given by [15, 63]:

$$C(\lambda_j, \lambda_k) = \frac{\sum_{i=1}^{N} [I_i(\lambda_j) - \bar{I}(\lambda_j)][I_i(\lambda_k) - \bar{I}(\lambda_k)]}{\sqrt{\sum_{i=1}^{N} [I_i(\lambda_j) - \bar{I}(\lambda_j)]^2} \cdot \sqrt{\sum_{i=1}^{N} [I_i(\lambda_k) - \bar{I}(\lambda_k)]^2}} \tag{4}$$

The numerator quantifies how their deviations from the respective means covary and the denominator normalizes this covariance by considering the standard deviations. PCC quantifies both the strength and direction of the linear relationship between two variables. In this particular case, it serves to quantify the extent of correlation among intensity fluctuations at different wavelengths. PCC values range from -1 to +1 indicating correlation strength, where -1 indicates a complete negative correlation, +1 represents a perfect positive correlation and 0 suggests no correlation. Here zero correlation means that the changes in one variable are not associated with any consistent changes in the other variable. In other words, the two variables are independent of each other. The diagonal line implies that every variable is perfectly correlated with itself (self-correlation) and the values along this diagonal will always be 1. A higher value of the correlation coefficient among intensity fluctuations at various wavelengths indicates a stronger linear relationship which implies that changes in the intensity fluctuations at one wavelength are more closely associated with changes in the intensity fluctuations at other wavelengths. In simpler terms, it suggests that the intensity fluctuations across different wavelengths are more synchronized. The PCC map serves as a heatmap plot, showing the correlation coefficients for all conceivable permutations of relevant wavelengths within the emission spectrum. The color

palette employed in this representation with varying intensity or magnitude features a spectrum of colors transitioning from blue to green, then to yellow and ultimately to red, producing a visual akin to a rainbow. Typically, positive correlations are depicted by an array of colors, including red, yellow and green with the intensity of these colors denoting the strength of the positive correlations. On the other hand, pale blue hues are indicative of a lack of correlation. The correlation coefficients are translated into heatmap plots, with each cell within the plot denoting the correlation between two specific wavelengths. These visualizations showed a range of colors to effectively convey both the intensity and direction of these cross-correlations. A previously reported work provides a comprehensive account of the mode-locking transition in RLs, supported by both experimental and numerical evidence [66]. Within this framework, the concept of incoherent emission is characterized as an outcome of a multitude of spatially overlapping resonances, which in turn leads to a highly correlated emission pattern.

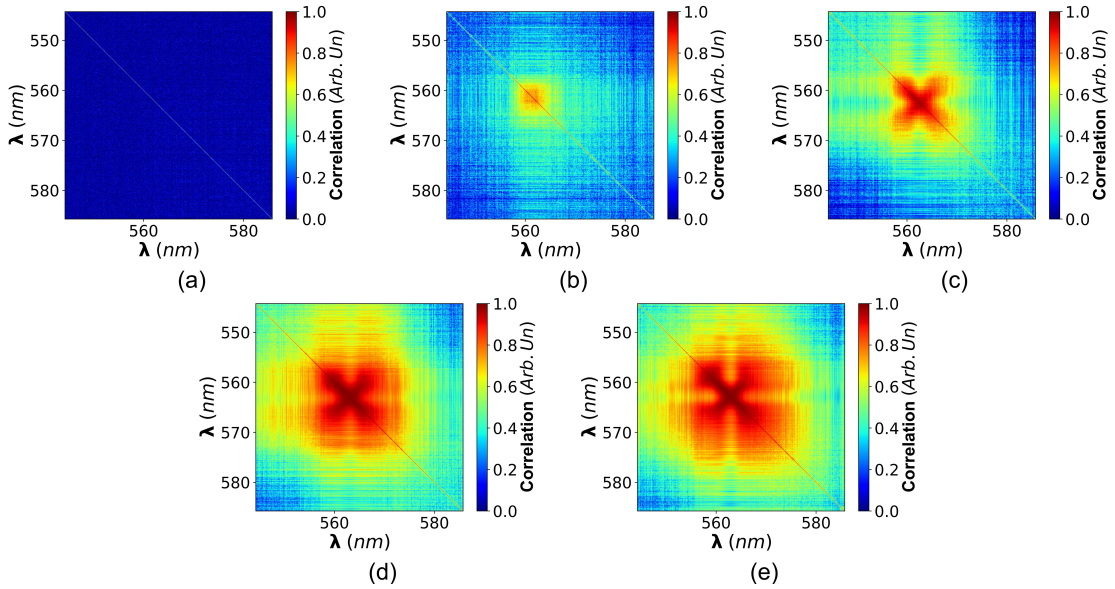

Figure 3: Heatmaps illustrating PCCs, revealing intensity fluctuations in the spectral data under different excitation energies: 13 μJ per pulse, 25 μJ per pulse, 40 μJ per pulse, 406 μJ per pulse and 577 μJ per pulse, shown in a, d, g, j and m respectively.

Recent studies have explored the application of Pearson's correlation coefficient in various fields, including the analysis of mode intensity correlations in nanofiber RLs. For instance, Montinaro et al. (2017) utilized Pearson's correlation to assess the intensity fluctuations at different wavelengths in RLs [67]. They found that the correlation coefficients were significantly larger in systems with waveguiding filaments compared to those with scattering nanoparticles [66], indicating a higher degree of mode intensity correlation in the former. in the analysis of the hybrid electronically addressable random (HEAR) laser, a modified Pearson coefficient was introduced to study intensity fluctuations and replica symmetry breaking (RSB) behavior [68]. This adaptation combines the Parisi overlap parameter with the standard Pearson coefficient, enabling a nuanced analysis of correlations in intensity fluctuations across different wavelengths. Sciuti et al. studied RLs using Rhodamine B-doped PMMA nanofibers produced via electrospinning, where PCC was utilized to analyze the temporal evolution of emission spectra [63]. This approach enabled a deeper understanding of mode competition and spectral shifts, offering insights into both coherent and incoherent RL emissions. Such applications demonstrate PCC's utility in tracking changes in complex systems, making it a valuable tool for developing sensors and monitoring

environmental changes. Jiangying et al. used Pearson correlation to analyze mode interactions in FRET-assisted random lasers (FRET-RL) [49]. Below the lasing threshold, intensity fluctuations were uncorrelated, but near the threshold, FRET-RL exhibited strong cross-correlations due to competition between modes, leading to disordered behavior and Replica Symmetry Breaking (RSB). In contrast, non-transferred random lasers (NTRL) showed distinct correlation bands with mode-locking effects, stabilizing quasimode interactions and favoring Gaussian statistics. A recent study on RLs using dye-doped colloidal potassium sodium niobate (KNN) nanoparticles found that Pearson correlation coefficients effectively illustrated the transition from weak to strong correlations in intensity fluctuations as excitation energy increased [15]. The study observed that the majority of modes had correlation coefficients below 0.5, indicating non-overlapping spatial modes.

Fig. 3 shows the heatmap plots that effectively illustrate the evolving correlation patterns with various energy regimes. In the prelasing phase (Fig. 3a), characterized at below the threshold (13 μJ per pulse), the heatmap is mostly blue which indicates a lack of correlation between different wavelengths. As the pump energy increases to around 25 μJ per pulse, small positive correlations emerge in the heatmap, visible as a central orange spot. This marks the onset of spontaneous emission, where the fluctuations in intensity begin to display some level of synchronization, although they remain weak compared to the lasing state. The correlation at this stage is attributed to broad, spontaneous emission (Fig. 3b). Spectra below the lasing threshold generally show these blue patterns, suggesting that intensity fluctuations at different wavelengths are not strongly correlated in this state. Consistently, the unimodal $P(q)$, with their centers located at $q_{max} = 0$ as illustrated in Fig. 1a and Fig. 1c, suggest the existence of replica symmetric paramagnetism. Around the threshold energy of 40 μJ per pulse, the heatmap (Fig. 3c) reveals more distinct patterns with larger positive correlations, shown in orange and red hues at the center. This indicates that the system is transitioning into lasing, where the intensities at different wavelengths start becoming more correlated. For energies well above the threshold (406 μJ per pulse and 577 μJ per pulse), the heatmap plots in Fig. 3d and Fig. 3e, the correlation patterns become even more pronounced, with widespread orange and red regions in the heatmap. Correspondingly RSB phenomenon emerged around the threshold supported by the presence of side peaks in the bimodal $P(q)$ as shown in Figs. 1e, 1g and 1i. The heatmap shows a dark red diagonal line, indicating perfect correlation among modes at the same wavelength. Additionally, in the case of incoherent RL, a prominent red region across the central emission wavelength bands is observed, indicating high levels of correlation among different wavelengths. This pattern suggests that the spectra are influenced by overlapping spatial features, implying a significant degree of spatial overlap among the emission modes. Specifically, the mean correlation coefficient for wavelengths within the emission band in the incoherent RL is ≈ 0.9, underscoring a strong correlation across the lasing spectrum. This, in turn, suggests that incoherent RLs are not modeless, but rather the modes are spatially overlapped.

3.4 Fluctuation Regimes

The same dataset was used to compute the α exponent values by fitting the peak intensities using the alpha stable distributions. It is essential to consider the Generalized Central Limit Theorem,

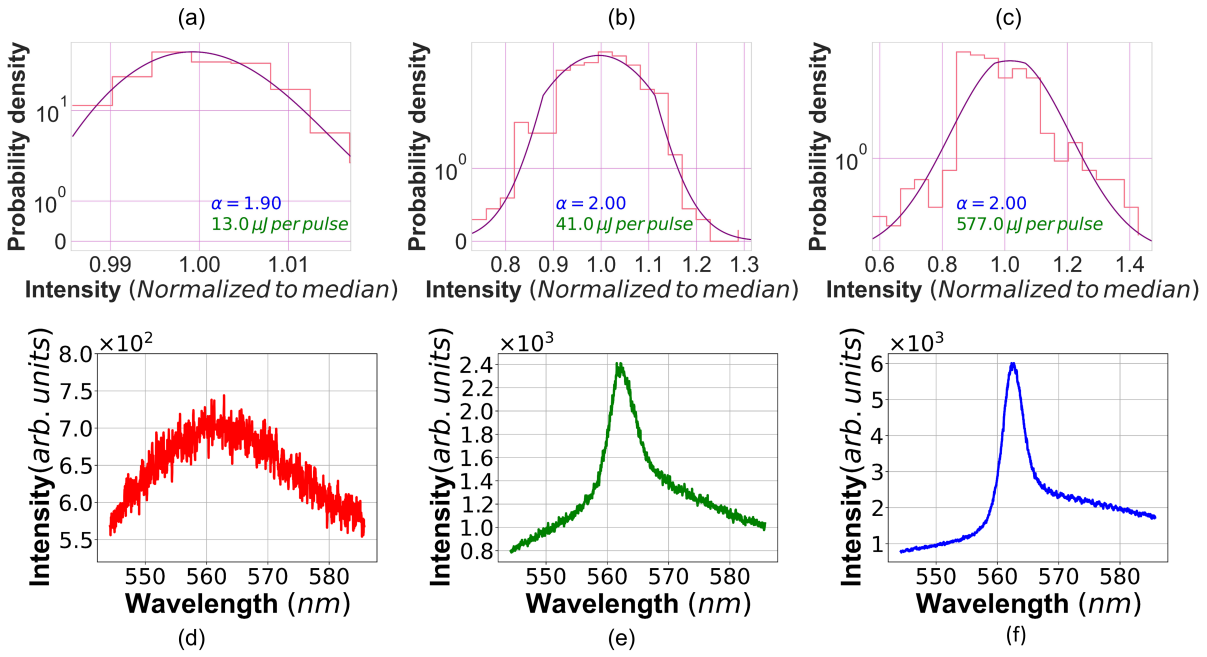

Figure 4: Distribution of peak intensities for different excitation energies, (a) 13.0 μJ per pulse, (b) 41.0 μJ per pulse, (c) 577.0 μJ per pulse with solid purple curves indicating fits to the α-stable distribution. The corresponding spectrum is given in d, e and f respectively.

especially when confronted with significant deviations from Gaussian behavior which is often induced by strong fluctuations. This theorem posits that the sum of random variables converges to an α-stable distribution with an α value less than 2. Notably, rare and significant events, such as the emergence of random peaks on a broad background of spontaneous emission within a narrow spectral range, contribute to a dataset characterized by substantial variance in the context of temporally coherent RLs. In the context of studying statistical fluctuations in RL spectra, two primary approaches are available for each set of spectra or data points. The first approach involves fitting only the tail of the peak intensity histogram with a power law distribution and the second approach entails fitting the entire dataset with an α-stable distribution. It is worth noting that while the first approach is valid, it relies on only a few of the largest values. Hence a substantial number of spectra is required to draw meaningful statistical conclusions. The latter method is considered more accurate as it utilizes all available data points and provides a comprehensive analysis of the fluctuations. Accurately capturing the tail behavior of Lévy flight distributions is challenging with limited measurements, particularly when the α parameter approaches 2. Distinguishing between a Gaussian distribution and Lévy requires a subjective assessment and therefore, a threshold value is set at α=1.8. Beyond this, the characteristics of the intensity distribution and emission spectra transition towards Gaussian behavior [69]. The modes in RL systems can be treated as random variables and regression algorithms are strong candidates to estimate parameters related to them. Hence, MLE is adopted to determine the parameters of the α-stable distribution [70, 15]. Incoherent emissions characterized by shot-to-shot fluctuations in intensity were encountered throughout the experiment. The α-stable Lévy distribution is fitted to the histogram of peak intensities, with a focus on fluctuations near the central maxima. The results shown in Fig. 4a to Fig. 4c illustrate the statistical regimes of fluctuations (well below, around and far above the threshold) with the α values clearly indicated in the inset.

Importantly, the observations revealed α values ranging between 1.8 and 2, representing the statistical characteristics of these fluctuations. There is no occurrence of Lévy fluctuations in the proximity of the threshold and all fluctuation regimes adhered to Gaussian characteristics. The reason for this behavior is that all the fluctuations clustered around a mean value implying finite variance signifying the persistence of Gaussian statistics in this scenario. Fig. 4d to Fig. 4f shows the corresponding spectra.

Fig. S2 shows the variation of the α index and magnitude of q_{max} in response to the changes in pump energy. The RSB glassy phase is evident here and the initiation of the Lévy statistical characteristic remains absent. The α values pertained to the range of 1.9 to 2, specifically concerning the incoherent and narrowly distributed spectral emissions from dye-Kaolinite RLs. It is in agreement with the literature where the appearance of the RSB transition is associated with the RL threshold, regardless of the presence or absence of the Lévy regime [40].

3.5 Speckle-free imaging of a TEM grid

Speckles are coherent artifacts that are caused by intense reflections and scattering from sample surfaces due to the high spatial and temporal coherence of lasers. It can deteriorate image quality significantly by creating a grainy interference pattern. While effective imaging techniques like Optical Coherence Tomography (OCT) and multiphoton imaging exist, they often come at a high cost and require specialized expertise. RLs offer a solution by providing low spatial coherence, thereby reducing speckles and enhancing image quality [60, 71, 59, 72, 61, 73, 51, 74, 56, 58]. RLs have versatile applications in bioimaging [75–78], holography [79], as well as OCT [80, 81]. They provide several advantages, including non-contact imaging, technical simplicity and the capability to provide high contrast and high-resolution images at a comparatively lower cost. Traditional wide-field microscopes often rely on broadband and incoherent light sources such as LEDs and xenon lamps, resulting in images with lower contrast. The lack of a specific optical cavity and optic axis in RL systems allow any mode to propagate in any direction and contribute to overall lasing resulting in low coherence. Thus, RLs have low spatial coherence, quasi-monochromatic emissions and tunable scattering properties. These unique attributes make them particularly well-suited for bioimaging, holography and OCT. Redding et al. reported minimal speckle formation with RL illumination [60].

Emission from R6G-Kaolinite RL are used to capture speckle-free images of a TEM grid, demonstrating reduced distortion and enhanced clarity using the experimental setup shown in Fig. 5. In this optical system, the RL light source is directed onto the object (a TEM grid) using a lens (L1) and an objective (Obj). The output light from the object is imaged by a camera ($Neo\ sCMOS$, $Andor$) using imaging optics (combination of lenses represented as L2). Four different light sources were employed: a 532 nm laser, the emission from the R6G-Kaolinite system below threshold, the emission from the same system around threshold, and the RL emission produced above threshold. The resulting images of the TEM grid were compared. The resulting images of the TEM grid were compared. The images are pseudo-colored using $ImageJ$, allowing precise visualization of the speckle reduction. The speckle contrast (C) is calculated to assess the spatial

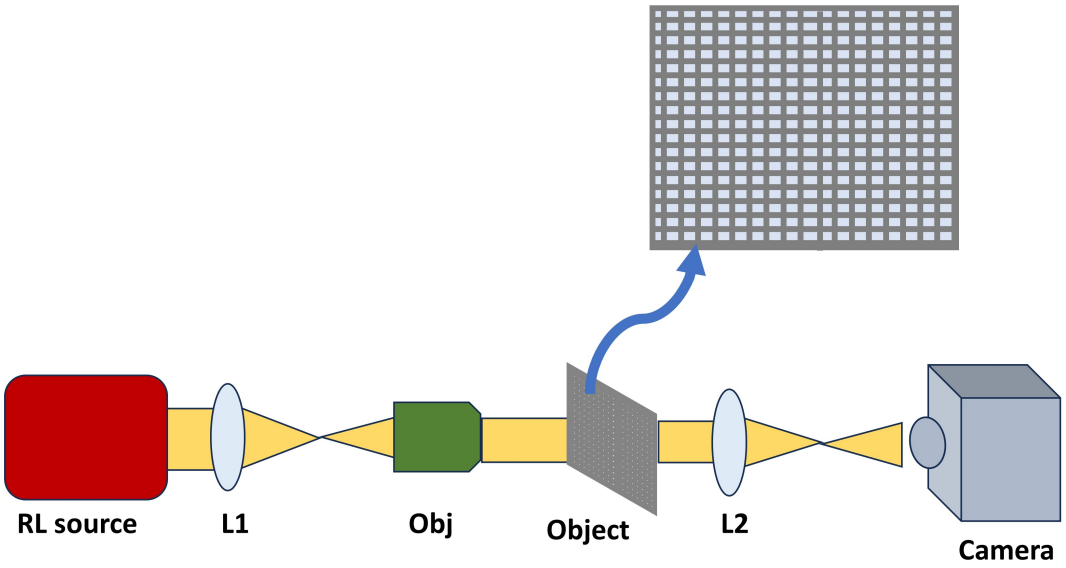

Figure 5: Experimental setup for speckle-free imaging. L:Lens and Obj:Objective.

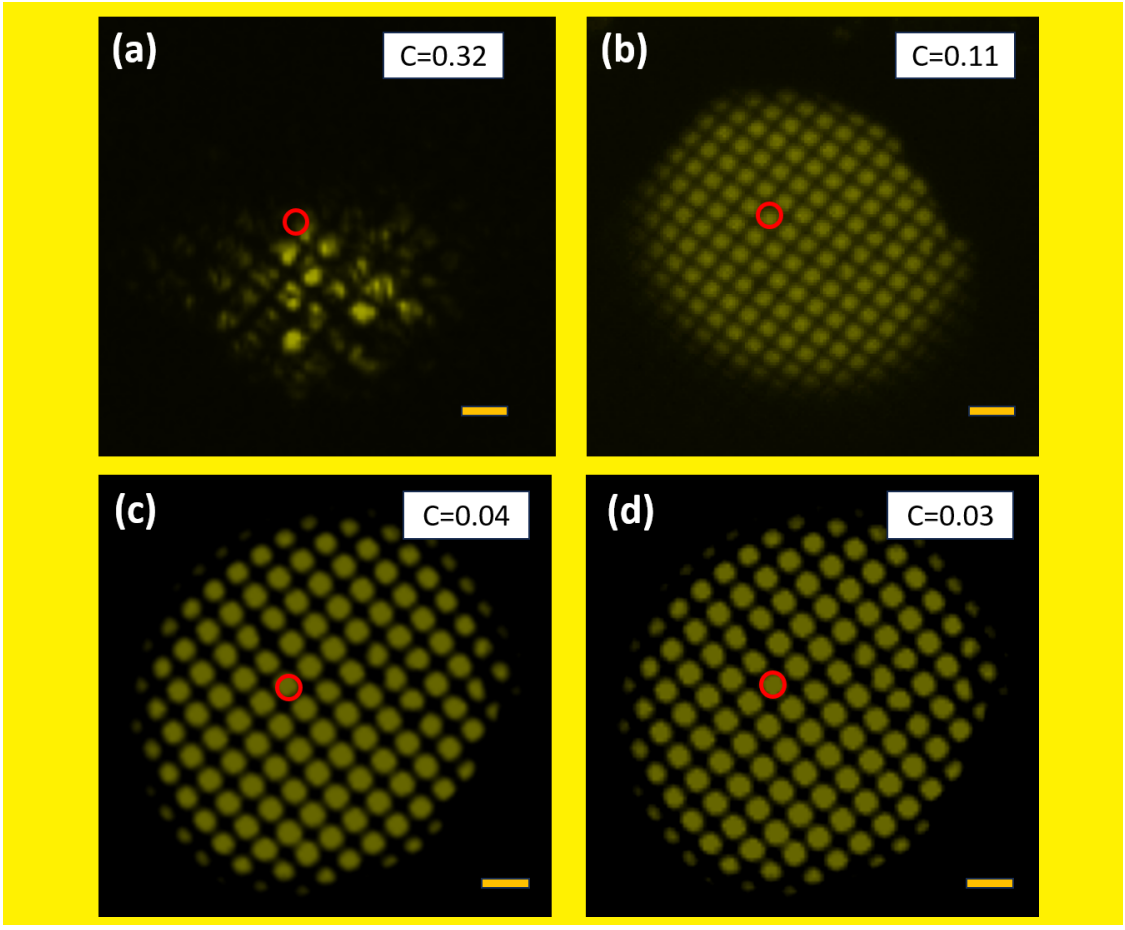

Figure 6: Images of a TEM grid using (a) laser, (b) below threshold and (c) around threshold and above threshold of dye Kaolinte emission.

coherence by using the following equation [59, 82, 60, 83]:

$$C = \frac{\sigma_I}{\langle I \rangle} \tag{5}$$

where σ_I represents the standard deviation and $\langle I \rangle$ is the average intensity of the image. C=1 signifies total spatial coherence and C=0 indicates spatial incoherence. The speckle contrast values for the previously mentioned light sources (532 nm laser, below threshold, around threshold, and above threshold emission) have been quantified. The speckle contrast of the image taken with the laser is significantly higher (0.32) compared to that obtained with below threshold (0.11), around threshold (0.04), and above threshold (0.03) illumination, as shown in Fig. 6a, Fig. 6b, Fig. 6c and Fig 6d respectively. The speckle contrast value of the emission around the threshold is close to that of the emission above the threshold, indicating their similarity in speckle reduction performance.

4 Conclusion

In conclusion, this report investigated the possibilities of RLs, specifically utilizing a colloidal system featuring R6G dye in methanol and Kaolinite nanoclay scatterers to create a disordered active medium. The investigation extended to the intriguing phenomena of RSB and checking the potential presence of Lévy or Gaussian statistics in the context of fluctuations in the intensity of incoherent RLs. The presence of RSB within the RL system is identified without any indications of Lévy flight. The absence of Lévy behavior can be attributed to the tendency of fluctuations to cluster around a mean value, signifying finite variance. This particular attribute elucidates the continued prevalence of Gaussian statistics in this context. The functionalities of the present RL systems to successfully attain speckle-free imaging of a TEM grid are explored. This experiment outlines the practical utility and vast potential of RLs for applications such as imaging and beyond. The current investigation, therefore, represents a substantial contribution to advancing both the theoretical understanding and practical applications of the R6G-Kaolinite RL system across diverse domains.

5 Revision

Acknowledgement

We acknowledge the financial support from DST-Govt. of India for funding through INSPIRE scheme, CRS program of UGC-DAE CSR, Kolkata Centre (UGC-DAE-CSR-KC/CRS/19/ RC08/0485), India, SERB: CRG (Grant No. CRG/2021/001506), UGC-Govt. of India for funding through the Innovative Program and Special Assistance Program (SAP Grant Nos. F.530/12/DRS/2009; F.530/13/DRS II/2016), RUSA, UGC: Scheme for Promotion of Academic and Research Collaboration (SPARC Grant Nos. P930, P1400, P1429, P1460), DST: Nano Mission (Grant Nos. SR/NM/NS-1420-2014(C), SR/NM/NS-54/2009), DST: Fund for Improvement of S&T Infrastructure (FIST Grant No. SR/FST/P SI-143/2009), DAE-Board of Research in Nuclear Sciences (BRNS Grant No. 39/29/2015-BRNS/39009), and DST Promotion of University Research and Scientific Excellence (PURSE Grant No. SR/S9/Z-23/2010/22(C, G)), Government of India programs for providing the facilities for research and development in IIUCNN, MGU.

Bibliography

[1] V. Letokhov. Generation of Light by a Scattering Medium with Negative Resonance Absorption. *Soviet Journal of Experimental and Theoretical Physics*, 26(4):835, 1968.

[2] Anderson SL Gomes, André L Moura, Cid B de Araújo, and Ernesto P Raposo. Recent advances and applications of random lasers and random fiber lasers. *Progress in Quantum Electronics*, 78:100343, 2021.

[3] Jonathan Andreasen, AA Asatryan, LC Botten, MA Byrne, Hui Cao, Li Ge, Laurent Labonté, Patrick Sebbah, AD Stone, Hakan E Türeci, et al. Modes of random lasers. *Advances in Optics and Photonics*, 3(1):88–127, 2011.

[4] Diederik S Wiersma. The physics and applications of random lasers. *Nature physics*, 4(5):359–367, 2008.

[5] Hui Cao. Review on latest developments in random lasers with coherent feedback. *Journal of Physics A: Mathematical and General*, 38(49):10497, 2005.

[6] Nideesh Padiyakkuth, Sabu Thomas, Rodolphe Antoine, and Nandakumar Kalarikkal. Recent progress and prospects of random lasers using advanced materials. *Materials Advances*, 2022.

[7] Feng Luan, Bobo Gu, Anderson SL Gomes, Ken-Tye Yong, Shuangchun Wen, and Paras N Prasad. Lasing in nanocomposite random media. *Nano Today*, 10(2):168–192, 2015.

[8] BD Urmanov, MS Leanenia, GP Yablonskii, OB Tagiev, and EG Asadov. Random lasers based on mixtures of micropowders of zncdsse solid solutions and phosphors ca4ga2s7: Eu2+ and ca (al0. 1ga0. 9) 2s4: Eu2+. *Journal of Applied Spectroscopy*, pages 1–4, 2023.

[9] Josivanir G Câmara, Davinson M Da Silva, Luciana RP Kassab, and Cid B De Araujo. Random laser emission from neodymium doped alumina lead–germanate glass powder. *Applied Optics*, 62(8):C59–C63, 2023.

[10] A Yu Pyatyshev, AV Skrabatun, AI Vodchits, AV Larkina, IA Khodasevich, and VA Orlovich. Picosecond random raman lasing in the spectral range of 360–630 nm using powders of potassium, sodium and strontium nitrates. *Laser Physics Letters*, 20(2):025401, 2023.

[11] Dongqing Lin, Yang Li, He Zhang, Shuai Zhang, Yuezheng Gao, Tianrui Zhai, Shu Hu, Chuanxiang Sheng, Heng Guo, Chunxiang Xu, et al. In situ super-hindrance-triggered multilayer cracks for random lasing in π-functional nanopolymer films. *Research*, 6:0027, 2023.

[12] Yanli Shen, Bingrong Shi, Jian Zhao, Hao Lv, Maorong Wang, Shuaiyi Zhang, Xia Wang, and Zhenjiang Li. Random laser emission from dye-doped polymer films enhanced by sic nanowires. *Journal of Physics D: Applied Physics*, 56(24):245101, 2023.

[13] Nideesh Padiyakkuth, Rodolphe Antoine, and Nandakumar Kalarikkal. Electrospun polyvinylidene fluoride mats as a novel platform for dye-doped random lasing. *Journal of Luminescence*, 252:119296, 2022.

[14] Nideesh Padiyakkuth, Rodolphe Antoine, and Nandakumar Kalarikkal. Random lasing in rhodamine 6g dye-kaolinite nanoclay colloids under single shot nanosecond pumping. *Optical Materials*, 129:112408, 2022.

[15] PK Nideesh, CS Chitra Lekha, R Antoine, and N Kalarikkal. Photonic replica symmetry breaking glassy transition and lévy flight statistics of emission intensity in dye-doped colloidal potassium sodium niobate random laser. *Optics & Laser Technology*, 169:110038, 2024.

[16] Arindam Dey, Ashim Pramanik, Koushik Mondal, Subrata Biswas, Udit Chatterjee, Fabrizio Messina, and Pathik Kumbhakar. Replica symmetry breaking in a colloidal plasmonic random laser with gold-coated triangular silver nanostructures. *Optics Letters*, 48(15):4141–4144, 2023.

[17] Randal C Polson and Z Valy Vardeny. Random lasing in human tissues. *Applied physics letters*, 85(7):1289–1291, 2004.

[18] Yu Wang, Zhuojun Duan, Zhu Qiu, Peng Zhang, Jianwei Wu, Dingke Zhang, and Tingxiu Xiang. Random lasing in human tissues embedded with organic dyes for cancer diagnosis. *Scientific reports*, 7(1):8385, 2017.

[19] Dingke Zhang, Yu Wang, Jun Tang, and Haixi Mu. Random laser marked plcd1 gene therapy effect on human breast cancer. *Journal of Applied Physics*, 125(20), 2019.

[20] Neda Ghofraniha and Claudio Conti. Spin glass behavior of random lasers: Experiments. In *Lévy Statistics and Spin Glass Behavior in Random Lasers*, pages 129–170. Jenny Stanford Publishing, 2023.

[21] Iván RR González, Ernesto P Raposo, Antônio MS Macêdo, Leonardo de S. Menezes, and Anderson SL Gomes. Coexistence of turbulence-like and glassy behaviours in a photonic system. *Scientific Reports*, 8(1):17046, 2018.

[22] Iván R Roa González, Bismarck C Lima, Pablo IR Pincheira, Arthur A Brum, Antônio MS Macêdo, Giovani L Vasconcelos, Leonardo de S. Menezes, Ernesto P Raposo, Anderson SL Gomes, and Raman Kashyap. Turbulence hierarchy in a random fibre laser. *Nature Communications*, 8(1):15731, 2017.

[23] Leonardo de S Menezes and Anderson SL Gomesb. Floquet spin-glass phase in a random fiber laser. 2023.

[24] N Ghofraniha, I Viola, F Di Maria, G Barbarella, G Gigli, L Leuzzi, and C Conti. Experimental evidence of replica symmetry breaking in random lasers. *Nature communications*, 6(1):6058, 2015.

[25] Jacopo Niedda. Realistic model for random lasers from spin-glass theory. *arXiv preprint arXiv:2306.08972*, 2023.

[26] Marc Mézard, Giorgio Parisi, and Miguel Angel Virasoro. *Spin glass theory and beyond: An Introduction to the Replica Method and Its Applications*, volume 9. World Scientific Publishing Company, 1987.

[27] Giorgio Parisi. Infinite number of order parameters for spin-glasses. *Physical Review Letters*, 43(23):1754, 1979.

[28] Hidetoshi Nishimori. *Statistical physics of spin glasses and information processing: an introduction*. Number 111. Clarendon Press, 2001.

[29] Giorgio Parisi. The order parameter for spin glasses: a function on the interval 0-1. *Journal of Physics A: Mathematical and General*, 13(3):1101, 1980.

[30] Patrick Charbonneau, Enzo Marinari, Giorgio Parisi, Federico Ricci-tersenghi, Gabriele Sicuro, Francesco Zamponi, and Marc Mezard. *Spin Glass Theory and Far Beyond: Replica Symmetry Breaking after 40 Years*. World Scientific, 2023.

[31] Daniel L Stein. Spin glasses. *Scientific American*, 261(1):52–61, 1989.

[32] Danijela Marković, Alice Mizrahi, Damien Querlioz, and Julie Grollier. Physics for neuromorphic computing. *Nature Reviews Physics*, 2(9):499–510, 2020.

[33] Bernhard H Korte, Jens Vygen, B Korte, and J Vygen. *Combinatorial optimization*, volume 1. Springer, 2011.

[34] S. Basak, A. Blanco, and C. López. Large fluctuations at the lasing threshold of solid- and liquid-state dye lasers. *Scientific Reports*, 6, 2016.

[35] Anirban Sarkar, BN Shivakiran Bhaktha, and Jonathan Andreasen. Replica symmetry breaking in a weakly scattering optofluidic random laser. *Scientific Reports*, 10(1):2628, 2020.

[36] Anirban Sarkar and BN Shivakiran Bhaktha. Replica symmetry breaking in coherent and incoherent random lasing modes. *Optics Letters*, 46(20):5169–5172, 2021.

[37] L Angelani, C Conti, G Ruocco, and F Zamponi. Glassy behavior of light. *Physical review letters*, 96(6):065702, 2006.

[38] Rafi Weill, Amir Rosen, Ariel Gordon, Omri Gat, and Baruch Fischer. Critical behavior of light in mode-locked lasers. *Physical review letters*, 95(1):013903, 2005.

[39] Pablo IR Pincheira, Andréa F Silva, Sandra JM Carreño, Serge I Fewo, André L Moura, Ernesto P Raposo, Anderson SL Gomes, and Cid B de Araújo. Replica symmetry breaking in random lasers based on colloidal rh-6g and specially designed tio2 nanoparticles. In *Frontiers in Optics*, pages FTu2G–3. Optica Publishing Group, 2016.

[40] Federico Tommasi, Emilio Ignesti, Stefano Lepri, and Stefano Cavalieri. Robustness of replica symmetry breaking phenomenology in random laser. *Scientific reports*, 6(1):1–8, 2016.

[41] Divya Sharma, Hema Ramachandran, and N Kumar. Lévy statistical fluctuations from a random amplifying medium. *Fluctuation and Noise Letters*, 6(01):L95–L101, 2006.

[42] Stefano Lepri, Stefano Cavalieri, Gian-Luca Oppo, and Diederik S Wiersma. Statistical regimes of random laser fluctuations. *Physical Review A*, 75(6):063820, 2007.

[43] Ravitej Uppu, Anjani Kumar Tiwari, and Sushil Mujumdar. Identification of statistical regimes and crossovers in coherent random laser emission. *Optics letters*, 37(4):662–664, 2012.

[44] Ravitej Uppu and Sushil Mujumdar. Lévy exponents as universal identifiers of threshold and criticality in random lasers. *Physical Review A*, 90(2):025801, 2014.

[45] Ravitej Uppu and Sushil Mujumdar. Exponentially tempered lévy sums in random lasers. *Physical review letters*, 114(18):183903, 2015.

[46] Pierre Barthelemy, Jacopo Bertolotti, and Diederik S Wiersma. A lévy flight for light. *Nature*, 453(7194):495–498, 2008.

[47] Anderson SL Gomes, Ernesto P Raposo, André L Moura, Serge I Fewo, Pablo IR Pincheira, Vladimir Jerez, Lauro JQ Maia, and Cid B de Araújo. Observation of lévy distribution and replica symmetry breaking in random lasers from a single set of measurements. *Scientific reports*, 6(1):27987, 2016.

[48] Bismarck C Lima, Anderson SL Gomes, Pablo IR Pincheira, André L Moura, Mathieu Gagné, Ernesto P Raposo, Cid B de Araújo, and Raman Kashyap. Observation of lévy statistics in one-dimensional erbium-based random fiber laser. *JOSA B*, 34(2):293–299, 2017.

[49] Jiangying Xia, Xiaojuan Zhang, Erlei Wang, Lei Hu, Tianyu Yang, Wenyu Du, Jiajun Ma, Kaiming Zhou, Lin Zhang, Kang Xie, et al. Replica symmetry breaking reveals the emission mechanism of fret-assisted random laser. *Journal of Lightwave Technology*, 2024.

[50] Xiaoyu Shi, Kaiyue Shen, Yaoxing Bian, Wanting Song, Jun Ruan, Zhaona Wang, and Tianrui Zhai. Programmable complex pumping field induced color-on-demand random lasing in fiber-integrated microbelts for speckle free imaging. *Science China Information Sciences*, 66(12):222401, 2023.

[51] Yilin Liu, Wenhong Yang, Shumin Xiao, Nan Zhang, Yubin Fan, Geyang Qu, and Qinghai Song. Surface-emitting perovskite random lasers for speckle-free imaging. *ACS nano*, 13(9):10653–10661, 2019.

[52] Sihao Huang, Siyu Dong, Zhengzheng Liu, Zijun Zhan, Qian Li, Zhiping Hu, Zeyu Zhang, Liang Wang, Jiajun Luo, Jiang Tang, et al. Random lasing from thermally evaporated quasi-two-dimensional perovskite film for speckle-free imaging. *ACS Photonics*, 11(4):1611–1618, 2024.

[53] Jun Wang, Jianqiang Qin, Zijun Zhan, Zhiping Hu, Sihao Huang, Fengxian Zhou, Qian Li, Zhengzheng Liu, Zeyu Zhang, Yuxin Leng, et al. Speckle-free imaging based on a quasi-2d perovskite random laser with a subwavelength thickness. *ACS Photonics*, 11(4):1664–1672, 2024.

[54] Wei Gao, Ting Wang, Jiangtao Xu, Ping Zeng, Wenfei Zhang, Yunduo Yao, Changsheng Chen, Mingjie Li, and Siu Fung Yu. Robust and flexible random lasers using perovskite quantum dots coated nickel foam for speckle-free laser imaging. *Small*, 17(39):2103065, 2021.

[55] Shanshan Wang, Weili Zhang, Ning Yang, Yandong Mou, and Yunjiang Rao. Speckle-free imaging using a high-power multimode random fiber laser. In *2021 IEEE 9th International Conference on Information, Communication and Networks (ICICN)*, pages 586–589. IEEE, 2021.

[56] Junhua Tong, Xiaoyu Shi, Lianze Niu, Xiao Zhang, Chao Chen, Liang Han, Shuai Zhang, and Tianrui Zhai. Dual-color plasmonic random lasers for speckle-free imaging. *Nanotechnology*, 31(46):465204, 2020.

[57] Yuan Wan, Zhihao Li, Zexu Liu, Yang Yang, Hongzhen Wang, Xianlong Liu, and Yangjian Cai. Robust speckle-free imaging using random lasers enhanced by tin nanoparticles in complex scattering environments. *Nanophotonics*, 12(23):4307–4317, 2023.

[58] Shih-Wen Chen, Jin-You Lu, Bing-Yi Hung, Matteo Chiesa, Po-Han Tung, Ja-Hon Lin, and Thomas Chung-Kuang Yang. Random lasers from photonic crystal wings of butterfly and moth for speckle-free imaging. *Optics Express*, 29(2):2065–2076, 2021.

[59] Arindam Dey, Ashim Pramanik, Partha Kumbhakar, Subrata Biswas, Sudip Kumar Pal, Sujit Kumar Ghosh, and Pathik Kumbhakar. Manoeuvring a natural scatterer system in random lasing action and a demonstration of speckle free imaging. *OSA Continuum*, 4(6):1712–1722, 2021.

[60] Brandon Redding, Michael A Choma, and Hui Cao. Speckle-free laser imaging using random laser illumination. *Nature photonics*, 6(6):355–359, 2012.

[61] Macarena Barredo-Zuriarrain, Ignacio Iparraguirre, Joaquín Fernández, Jon Azkargorta, and Rolindes Balda. Speckle-free near-infrared imaging using a nd3+ random laser. *Laser Physics Letters*, 14(10):106201, 2017.

[62] Hui Cao. Lasing in random media. *Waves in random media*, 13(3):R1, 2003.

[63] Lucas F Sciuti, Luiza A Mercante, Daniel S Correa, and Leonardo De Boni. Random laser in dye-doped electrospun nanofibers: study of laser mode dynamics via temporal mapping

of emission spectra using pearson's correlation. *Journal of Luminescence*, 224:117281, 2020.

[64] RV Ambartsumyan, NG Basov, PG Kryukov, and VS Letokhov. A laser with nonresonant feedback. *Sov. Phys. JETP*, 24:481–485, 1967.

[65] Pablo IR Pincheira, Andréa F Silva, Serge I Fewo, Sandra JM Carreño, André L Moura, Ernesto P Raposo, Anderson SL Gomes, and Cid B de Araújo. Observation of photonic paramagnetic to spin-glass transition in a specially designed tio 2 particle-based dye-colloidal random laser. *Optics Letters*, 41(15):3459–3462, 2016.

[66] Marco Leonetti, Claudio Conti, and Cefe Lopez. The mode-locking transition of random lasers. *Nature Photonics*, 5(10):615–617, 2011.

[67] Martina Montinaro, Vincenzo Resta, Andrea Camposeo, Maria Moffa, Giovanni Morello, Luana Persano, Karolis Kazlauskas, Saulius Jursenas, Ausra Tomkeviciene, Juozas V Grazulevicius, et al. Diverse regimes of mode intensity correlation in nanofiber random lasers through nanoparticle doping. *ACS Photonics*, 5(3):1026–1033, 2017.

[68] Edwin Coronel, Avishek Das, Iván RR González, Anderson SL Gomes, Walter Margulis, JP Von Der Weid, and Ernesto P Raposo. Evaluation of pearson correlation coefficient and parisi parameter of replica symmetry breaking in a hybrid electronically addressable random fiber laser. *Optics express*, 29(15):24422–24433, 2021.

[69] Emilio Ignesti, Federico Tommasi, Lorenzo Fini, Stefano Lepri, Vivekananthan Radhalakshmi, Diederik Wiersma, and Stefano Cavalieri. Experimental and theoretical investigation of statistical regimes in random laser emission. *Physical Review A*, 88(3):033820, 2013.

[70] José M Miotto, Holger Kantz, and Eduardo G Altmann. Stochastic dynamics and the predictability of big hits in online videos. *Physical Review E*, 95(3):032311, 2017.

[71] Manoj K Bhuyan, Antonin Soleilhac, Madhura Somayaji, Tatiana E Itina, Rodolphe Antoine, and Razvan Stoian. High fidelity visualization of multiscale dynamics of laser-induced bubbles in liquids containing gold nanoparticles. *Scientific Reports*, 8(1):9665, 2018.

[72] Tzu-Hsuan Yang, Chun-Wei Chen, Hung-Chang Jau, Ting-Mao Feng, Chih-Wei Wu, Chun-Ta Wang, and Tsung-Hsien Lin. Liquid-crystal random fiber laser for speckle-free imaging. *Applied Physics Letters*, 114(19), 2019.

[73] Brandon Redding, Alexander Cerjan, Xue Huang, Minjoo Larry Lee, A Douglas Stone, Michael A Choma, and Hui Cao. Low spatial coherence electrically pumped semiconductor laser for speckle-free full-field imaging. *Proceedings of the National Academy of Sciences*, 112(5):1304–1309, 2015.

[74] Rui Ma, Yun Jiang Rao, Wei Li Zhang, and Bo Hu. Multimode random fiber laser for speckle-free imaging. *IEEE journal of selected topics in quantum electronics*, 25(1):1–6, 2018.

[75] R Gayathri, CS Suchand Sandeep, Venkata Siva Gummaluri, R Mohamed Asik, Parasuraman Padmanabhan, Balázs Gulyás, C Vijayan, and Vadakke Matham Murukeshan. Plasmonic random laser enabled artefact-free wide-field fluorescence bioimaging: uncovering finer cellular features. *Nanoscale Advances*, 4(10):2278–2287, 2022.

[76] R Gayathri, CS Suchand Sandeep, C Vijayan, and VM Murukeshan. Lasing from micro-and nano-scale photonic disordered structures for biomedical applications. *Nanomaterials*, 13(17):2466, 2023.

[77] R Gayathri, CS Suchand Sandeep, C Vijayan, and VM Murukeshan. Wide-field microscopic structural imaging of biological tissues using random laser. In *European Conference on Biomedical Optics*, pages ES1A–7. Optica Publishing Group, 2021.

[78] R Gayathri, CS Suchand Sandeep, K Ahmad, C Vijayan, and VM Murukeshan. Non-contact, artefact-free corneal imaging using random laser. In *Imaging Systems and Applications*, pages ITu1D–4. Optica Publishing Group, 2021.

[79] Subha Prakash Mallick and Zson Sung. Holographic image denoising using random laser illumination. *Annalen der Physik*, 532(12):2000323, 2020.

[80] B Karamata, P Lambelet, M Laubscher, RP Salathé, and T Lasser. Spatially incoherent illumination as a mechanism for cross-talk suppression in wide-field optical coherence tomography. *Optics letters*, 29(7):736–738, 2004.

[81] B Redding, MA Choma, and H Cao. Spatially incoherent random lasers for full field optical coherence tomography. In *CLEO: Science and Innovations*, page PDPC7. Optica Publishing Group, 2011.

[82] Zhendong Xie, Kang Xie, Taoping Hu, Jiajun Ma, Junxi Zhang, Rui Ma, Xusheng Cheng, Jianquan Li, and Zhijia Hu. Multi-wavelength coherent random laser in bio-microfibers. *Optics Express*, 28(4):5179–5188, 2020.

[83] Ashim Pramanik, Subrata Biswas, Partha Kumbhakar, and Pathik Kumbhakar. External feedback assisted reduction of the lasing threshold of a continuous wave random laser in a dye doped polymer film and demonstration of speckle free imaging. *Journal of Luminescence*, 230:117720, 2021.